

Optimal homogenization of perfusion flows in microfluidic bio-reactors; a numerical study

Fridolin Okkels, Martin Dufva, and Henrik Bruus

Department of Micro- and Nanotechnology, Technical University of Denmark,
DTU Nanotech, Building 345 East, DK-2800 Kongens Lyngby, Denmark

E-mail: fridolin.okkels@nanotech.dtu.dk

Abstract. To ensure homogeneous conditions within the complete area of perfused microfluidic bio-reactors, we develop a general design of a continuously feed bio-reactor with uniform perfusion flow. This is achieved by introducing a specific type of perfusion inlet to the reaction area. The geometry of these inlets are found using the methods of topology optimization and shape optimization. The results are compared with two different analytic models, from which a general parametric description of the design is obtained and tested numerically. Such a parametric description will generally be beneficial for the design of a broad range of microfluidic bioreactors used for e.g. cell culturing and analysis, and in feeding bio-arrays.

Submitted to: *J. Micromech. Microeng.*

PACS numbers: 87.85.M-, 02.60.Pn, 47.15.-x, 87.85.Va

1. Introduction

The development of microfluidics, to handle minute amounts of fluids, is currently revolutionizing fluid transport in the field of analytic cell-biology: Traditionally, cells are cultured in so-called batch cultures in a flask and an experiment is typically initiated by adding an agent. After a certain time, such as a day or two, the response of the agent is studied using typically only one reporter such as fluorescence. In order to increase throughput, cells can, at present, be cultured and assayed in robotically controlled 96 or 384 well plates. By contrast, culturing of cells on a microfluidics device gives a range of new possibilities [1] e.g. studying cell mobility in real time when exposed to stable continuous gradients [2]. Furthermore, combinatory experiments can be performed on chip that are based on arrays of interconnecting chambers [3, 4].

The inlet design presented in this paper introduces a number of improvements to current perfused bio-reactors: The creation of uniform flow conditions all over the bio-reactor ensures homogeneous cell conditions both with regards to concentrations of externally supplied growth-factors and to the shear induced on the cells by the perfusion flow. Too small a height of cell culture chips is inhibiting cell growth [5, 6, 7], and in Refs. [8, 9] it has been shown that the chamber height must exceed 1.5 mm in order to provide identical culturing conditions as in traditional cell culture flask. On the other hand, to ensure laminar flow conditions, a small height is preferred. Therefore in the case of cell-culturing chips, a chamber height of 1.5 mm is optimal. In other cases, such as for micro-array hybridization chambers, the functionality indeed benefits from far smaller reactor-channel heights, where volume needs to be minimized in combination with a maximization of reaction area.

In recent years different bio-reactors have been constructed, where the uniformity of the perfusion flow along the reaction area has been achieved at the expense of a large hydraulic resistance across the whole bio-reactor [3]. One example is the Micro cell-culture chamber by M. Stangegaard et al. [8], where the fluid is directed from a wide reservoir through a large number of small parallel channels. This barrier creates a large pressure drop which gives rise to the uniform flow. From the inlet structure described from this work, the same uniform flow-field can be achieved with a significantly lower pressure-drop. This opens up the possibilities of driving the perfusion flow by low-power methods such as e.g. buoyancy force, which recently has been used to drive other microfluidic devices [18].

Our novel design also reduces the fluid volume used in creating the uniform flow, which is crucial both when dealing with expensive biochemical samples or to avoid dilution of small samples. Additionally it will enable a better analysis of fast cell-reaction kinetics with high time resolution.

The paper is organized as follows: In section 2 the general bio-reactor layout is outlined together with an introduction of the related characteristic parameters. In section 3 the optimal structure of the perfusion inlet is found, first by the general method of topology optimization, which imposes no constraints on the topology of the

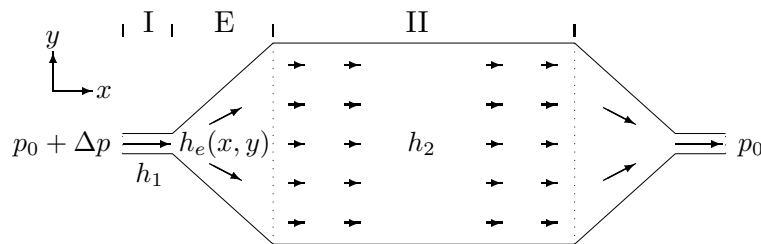


Figure 1. A sketch of the bio-reactor with its three sections: (I) the perfusion inlet of constant height h_1 , (E) the expansion chamber of spatially varying height $h_e(x, y)$, and (II) the main reactor area of constant height h_2 . The perfusion flow, driven by the pressure drop Δp , is indicated by arrows.

structure. The resulting structure is further refined by the method of shape optimization. The optimized geometry is in section 4 compared to two simple expansion design, while in section 5 the results are summarized in a design guide. The analysis and the design guide is further verified by full 3D simulations in section 6. A conclusion is given in sec. 7.

2. Geometry and basic flow equations of the microfluidic bio-reactor

The generic microfluidic bio-reactor layout used in this work is illustrated in figure 1. It consists of a single microchannel perfusion inlet (I) of constant height h_1 , which broaden out in an expansion chamber (E) of varying height $h_e(x, y)$ to distribute the fluid over the much wider and more shallow main reactor (II) of constant height h_2 , where the cells are immobilized. All vertical channel and chamber heights in the z direction are much smaller than any lateral length scale in the xy plane; the bio-reactor is thus flat.

The main objective is to obtain a uniform flow in the main reactor with minimal pressure drop Δp and with a minimal volume of the expansion chamber. This is achieved by carefully designing variations in chamber height $h_e(x, y)$ of the expansion chamber. As the constant inlet channel height h_1 is assumed larger than the constant height of the main reactor area h_2 , the height variation in the expansion chamber (E) will be bounded by these two heights:

$$h_1 \geq h_e(x, y) \geq h_2. \quad (1)$$

The whole bio-reactor is assumed symmetric both through a central vertical and a central horizontal axis, and as a consequence only the upper left part will be dealt with here.

As we consider only low concentrations of the solutes and a constant temperature, the density ρ and viscosity η of the buffer liquid are constant in space, and the flow is determined by the geometry of the reactor and the applied pressure drop Δp driving the flow. As a consequence of the assumed flatness of the bio-reactor, the pressure p does not vary in the vertical z direction, i.e. $\partial p / \partial z = 0$. Moreover, due to the small heights, viscous damping from the top and bottom plates of the bio-reactor dominates the fluid

flow and makes the flow laminar. This is evident from the value of the Reynolds number Re given the low flow velocities, $u \approx 1$ mm/s, and small length-scales, $h \approx 1$ mm of the system: $Re \approx 1$.

In this flow regime it is useful to work with the z -averaged 2D velocity field $\mathbf{u}(x, y) = (1/h(x, y)) \int_0^h \mathbf{v}(x, y, z) dz$ of the full 3D field $\mathbf{v}(x, y, z)$. To a good approximation \mathbf{u} fulfills the 2D Brinkman-Darcy equation [10],

$$\eta \nabla^2 \mathbf{u} - \frac{12\eta}{h^2(x, y)} \mathbf{u} - \nabla p(x, y) = \mathbf{0}. \quad (2)$$

Here the prefactor $12\eta/h^2(x, y)$, also denoted the damping coefficient α ,

$$\alpha = \frac{12\eta}{h^2(x, y)}, \quad (3)$$

is reminiscent of the z -part of the Laplace operator in the full 3D-description, and it represents the dominant part of the viscous damping of the liquid in the system.

For possible continues changes in the height $h(x, y)$ of the expansion region (E), the z -averaged 2D velocity field is not divergence-free due to mass-conservation, but an additional term arises: $\nabla \cdot \mathbf{u}(x, y) = -|\nabla h(x, y)|/h(x, y)$. In the case of possible discontinues jumps in height along an interface, this correction becomes the following new boundary condition on the interface:

$$h_1 \mathbf{u}_1 \cdot \mathbf{n} = h_2 \mathbf{u}_2 \cdot \mathbf{n}, \quad \mathbf{u}_1 \cdot \mathbf{t} = \mathbf{u}_2 \cdot \mathbf{t}, \quad p_1 = p_2, \quad (4)$$

where the height-subscript is extended to the corresponding velocities and pressures.

Working with the 2D-restricted description, the detailed geometry of the expansion chamber is illustrated in figure 2. The important in-plane length scales are the length L of the expansion chamber, the width W of the main reactor, and the width ℓ of the inlet. To achieve a uniform flow in the main chamber, the pressure along the line A dividing the expansion chamber and the main chamber must be constant. Consequently, the spatial variation of the expansion chamber height $h_e(x, y)$ must be optimized in order to get as homogeneous pressure along line A as possible.

3. Optimization

To enable optimization of the system two additional parts are introduced. First, a set of design variables $\boldsymbol{\gamma}$, which uniquely characterizes all available configurations in the optimization problem, and for which a unique solution $\mathbf{U}(\boldsymbol{\gamma})$ to the system exists. Second, an objective function Φ which quantifies how well a given configuration of the system performs. By convention Φ has to be minimized in order to achieve the optimal solution, and generally the objective function can depend on the design variables and the related solution of the system $\Phi = \Phi(\boldsymbol{\gamma}, \mathbf{U}(\boldsymbol{\gamma}))$.

As alluded to in the previous section, we base our objective function on the homogeneity of the pressure along the cross-section A, since a uniform pressure there will lead to the required uniform flow field in the main reactor. In the following, this objective will be expressed in two different ways, depending on the given optimization methods.

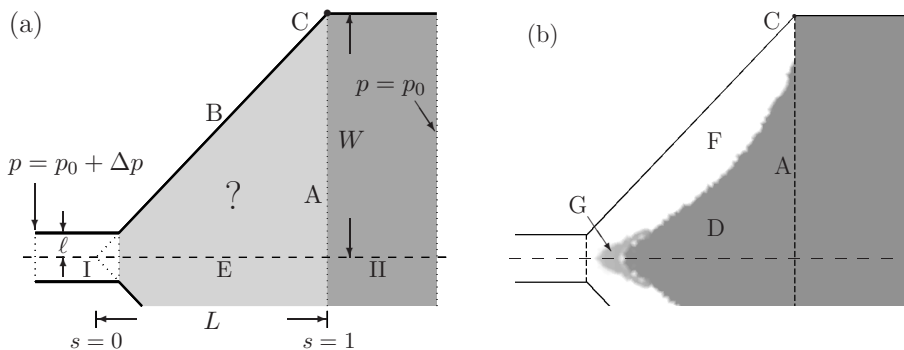


Figure 2. (a) The geometry of the expansion chamber E. The parameters related to geometry and flow are defined together with specific segments and points used for later reference. The optimal transition between the inlet height h_1 (white area) and the main reactor channel height h_2 (gray) occurs inside the expansion region E (light gray). (b) Topology optimized height variation in the expansion region. The height changes almost step-like from the white region F (h_1) to the gray region D (h_2). Note the small region of intermediate height marked G.

3.1. Topology optimization of the spatial height variation

To search for the globally optimal solution, and not a priori exclude any non-intuitive solutions, we will not rely on any pre-described variation of the height. Therefore, we begin by applying the method topology optimization [12], which by definition is independent of the topology and therefore unlimited in its search for the optimal bio-reactor design. The method of topology optimization was first applied to the field of structural mechanics[13], and have been recently implemented to the field of microfluidic systems [11, 14] and chemical microreactors [15].

Arbitrary height variations of $h_e(x, y)$ can be realized by representing the height as a variation of the design variable field $\gamma(x, y)$, where $0 \leq \gamma \leq 1$. To cover the range of heights defined in equation (1), the design variable is assigned the value $\gamma = 0$ to describe chamber heights equal to the inlet height h_1 and the value $\gamma = 1$ for heights equal to the main reactor height h_2 . In the expansion chamber, now denoted the design region Ω , the design field can take any value $0 \leq \gamma(x, y) \leq 1$ to describe all possible height variations $h_e(x, y)$.

The actual implementation, method and procedure of topology optimization will not be touched upon here, as it is fully described in the work of Olesen, Okkels and Bruus [14]. Still what is essential for this work is the objective function Φ , which has to be chosen with care. To obtain a numerically stable search we define Φ as the square deviation of the pressure around a reference pressure p_{ref} along A:

$$\Phi = \frac{1}{W} \int_A (p - p_{\text{ref}})^2 ds. \quad (5)$$

We choose p_{ref} as the pressure at the far corner C in the case where the expansion chamber has the same height h_1 everywhere as the inlet.

Figure 2(b) shows the resulting optimal height distribution $h_e(x, y)$ for the following set of parameters: $W = 10^{-2}$ m, $L = 0.95 W$, $\ell = 0.1 W$, $h_1 = 0.04 W$, and $h_2 = 0.02 W$,

where the gray-scale color-coding spans from height h_1 in white down to h_2 in gray. We define the ratio A between the two damping coefficients $12\eta/h_1^2$ and $12\eta/h_2^2$ as

$$\mathcal{A} = \left(\frac{h_1}{h_2}\right)^2, \quad (6)$$

and get the value of $\mathcal{A} = 4$ for figure 2(b).

As mentioned earlier, any change in height produces a correction-term to the continuity equation, when using a 2D-restricted description. It turns out that both ways of implementing this correction in the topology optimization problem fails, due to the very nature of the method. First, the free variations of the design field in topology optimization prohibits any interface to be defined a priori, and therefore the boundary conditions of equation (4) cannot be applied in this step of the optimization procedure. Second, it turns out that the solutions of the topology optimization problem involves sharp transitions in the height, limited by the grid-meshing length-scale of the finite element method. Therefore when including the correction-term to the continuity equation, a fluid source is added to single mesh-elements, and this destabilizes the convergence of the method. The way to work about this limitation, is to add the boundary conditions of equation (4) to the shape-optimization method, applied later in the optimization process, after the shape-optimization has been preliminarily compared to the topology-optimization.

From the topology optimized solution in figure 2(b) we see that among all possible height variations, the optimal design consists of a single sharp transition between a region of inlet height h_1 , and a region of main reactor height h_1 . Only very close to the inlet channel is seen an ambiguity which indicate the possible existence of a region of intermediate height. From topology optimizations for other parameter-values, similar solutions arise with a sharp transition between regions of height h_1 and h_2 , and consequently we conclude that such a single-connected transition is indeed the optimal solutions of the problem.

To evaluate the quality of the topology optimized solution, we plot in figure 3 the pressure contour lines of the solution in figure 2(b), including a contour line corresponding to the value $p = p_{\text{ref}}$ which goes through the corner C of the expansion chamber. Except close to the upper side wall, the pressure is seen to be uniform at the entrance of the main reactor, and it decreases uniformly throughout the whole extension of the main reactor.

The chosen parameters used for the solution in figures 2(b) and 3 represent a rather extreme case, i.e., a combination of a small height-difference $\mathcal{A} = 4$ and a wide expansion $L/W = 0.95$. As a result the transition extends nearly through the whole expansion region, but for all common parameters, the type of solution remains optimal.

From the results of the topology optimization it is therefore natural to proceed with the shape optimization method, which compared to topology optimization involves fewer design parameters, is faster, and is numerically more stable.

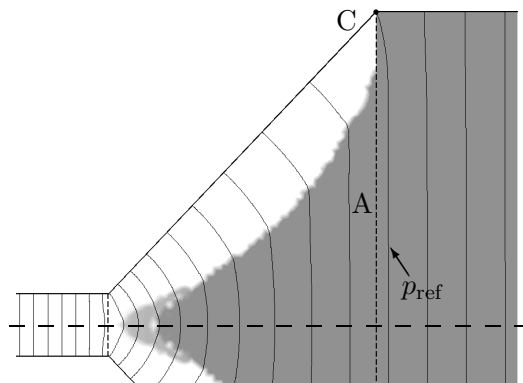


Figure 3. The contour lines of the pressure $p(x, y)$ in the topology optimized design. The contour $p = p_{\text{ref}}$, going through the corner C is marked.

3.2. Shape-optimization

In shape optimization the interface line between the heights h_1 and h_2 in the transition chamber is given by a cubic interpolation line through a number of control points $(x_i, y_i), i = 1, 2, \dots, N_\beta$ as shown in figure 4(a) with $N_\beta = 6$. It is convenient to parameterize the points by the expression

$$(x_i, y_i) = (s_i L, s_i \beta_i W), \quad \frac{\ell}{W} < s_i < 1, \quad 0 < \beta_i < 1, \quad (7)$$

which ensures that all points lie within the expansion chamber. By fixing the factors β_i by $\beta_i = [1 - 1/(3 N_\beta)] \times [(i - 1)/(N_\beta - 1)]$, a relatively even distribution of the control points is also ensured. During the optimization process the position of the interface line is changed by adjusting the control points s_i .

The optimization is carried out by a simplex-method relying only on values of the objective function $\Phi(\boldsymbol{\gamma})$, and not its partial derivatives $\partial\Phi/\partial\boldsymbol{\gamma}$. To ensure efficient convergence of the given simplex method, it is beneficial to assign initial values around unity for the design variables $\boldsymbol{\gamma}$. Furthermore, the method is unbound i.e. the design variables must give rise to a well-defined geometry regardless of their value. All this is accomplished by using the arcus tangent function:

$$s(\beta_i) = 1 - \gamma_0 (1 - \beta_i) \left\{ 1 + \frac{2}{\pi} \arctan \left[\frac{\pi}{2} (\gamma_i - 1) \right] \right\}, \quad i = 1 \dots N_\beta, \quad (8)$$

with

$$\boldsymbol{\gamma} = \{\gamma_0, \gamma_1, \dots, \gamma_{N_\beta}\}. \quad (9)$$

We use $N_\beta + 1$ design variables to determine N_β shape parameters because a faster convergence is achieved by adjusting the extend of the whole interface by a single parameter γ_0 . Furthermore, equation (8) let the initial configuration of

$$\boldsymbol{\gamma}_{\text{init}} = [\gamma_0, 1, \dots, 1] \quad (10)$$

give rise to a well-defined, straight interface line reaching from the position $(x, y) = ((1 - \gamma_0)L, 0)$ to the upper corner.

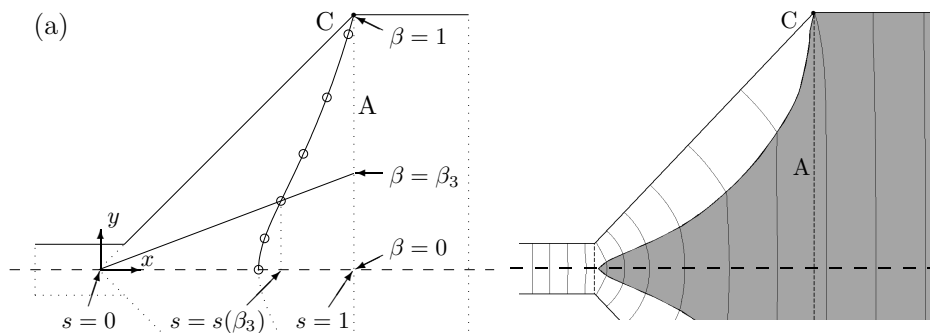


Figure 4. (a) Setup for the parametrization of the shape-optimization problem. Variables s and β parameterize the normalized x and y -axis respectively, and the control-points $s(\beta_i)$ are shown by circles with the interpolated interface curve in solid. (b) The pressure contours (thin lines) of the shape optimized positioning of the interface line $(s, s\beta)$ (thick line). Similarly to figure 3 the pressure contour are originating from the upper corner C

Now that the interface by definition extends to the upper corner, this constraint does not need to be included in the objective function Φ of the shape-optimization, and Φ can therefore be defined with the sole purpose of achieving a uniform pressure along segment A:

$$\Phi = \frac{1}{W} \int_A \left| \frac{\partial p}{\partial y} \right| ds. \quad (11)$$

The actual optimization of the design-variables follows two steps: First a rough initial interface is found by using the initial setup of equation (10), and only adjusting the single variable γ_0 , using a simple MATLAB implementation of a bounded golden section search with combined parabolic interpolation [19]. Once a suitable straight initial interface is found, the actual shape is obtained using a direct unbounded simplex search method, also implemented in MATLAB [20].

3.3. Results

First, the shape-optimization method has to be validated with respect to the topology optimized solution, shown in figures 2(b) and 3. The same parameter-values were used, and the resulting shape-optimization shown in figure 4(b), is indeed similar to figure 3. When comparing the results of the two optimization methods, it is observed that both the shape of the interface and the corner-pressure contour matches very well. Thereby we conclude that the shape-optimization is appropriate for the further analysis of the optimized interface.

Again it should be noted that the set of parameters used in figures 2(b), 3, and 4(b) is an extreme case, and therefore the shape-optimization method has been further tested to ensure the validity of this simple type of solutions.

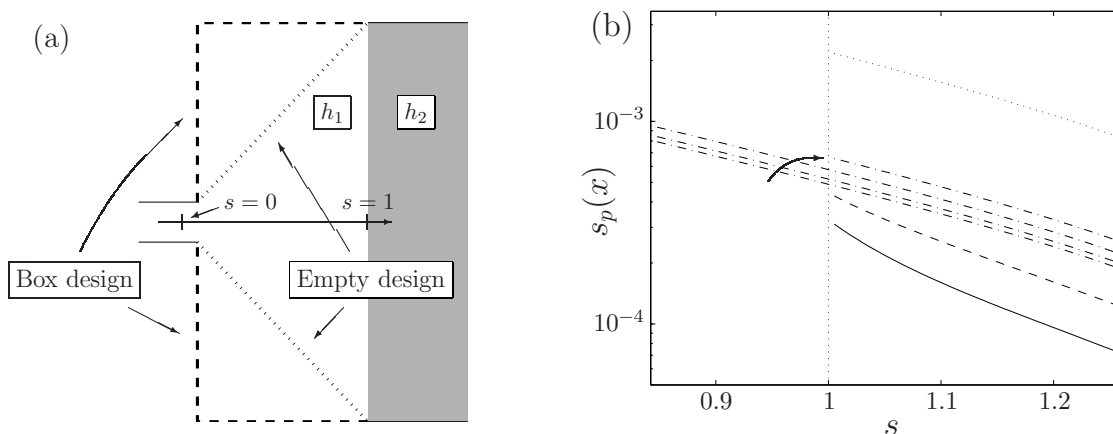


Figure 5. (a) A study of alternative expansion geometries. The expansion region in the *Empty design* is completely filled with inlet height h_1 , while the *Box design* has a simple box of height h_1 as expansion region. (b) Plot of the standard deviation $s_p(s)$ of the pressure vertically across the expansion region as a function of the normalized horizontal position s into the region, as seen in (a). The different curves are topology optimized (solid line), shape optimized (dashed line), empty design (dotted line), and the four types of box design (dot-dashed lines), where the arrow mark the order of the values $L = 0.35W, 0.55W, 0.75W, 0.95W$.

4. Comparison with alternative expansion geometries

Now that the design of the expansion region has been optimized, it is natural to compare its efficiency to other alternative expansion designs. The first obvious candidate is to uniformly fill the existing expansion region with height h_1 i.e. to remove the topology optimization distribution of height h_2 , and this we will call the *empty design*. The next design comes as we replace the expansion region with a simple box of width W and height h_1 , and this will be called the *box design*. Both alternative designs are shown in figure 5(a). To compare these new candidate designs to the optimized designs, we will measure the homogeneity of the pressure around the end of the expansion region. To get an quantitative measure of the homogeneity of the pressure in the first part of the reactor, we measure the standard deviation $\delta p(x)$ of pressure across the width along the y -axis of the reactor part for a fixed x -coordinate:

$$\delta p(x) = \sqrt{\langle [p(x, y) - \langle p(x, y) \rangle_y]^2 \rangle_y} \quad (12)$$

where $\langle \cdot \rangle_y$ is the mean along the y direction. Generally $\delta p(x)$ will decrease exponentially with the distance into the uniform reactor-part, and therefore $\delta p(x)$ will appear as an approximately straight line when shown in a log-linear plot as a function of x , see figure 5(b).

From the measurements presented in figure 5(b) it is first noted that both optimized designs produce a more homogeneous pressure-field than the alternative designs. While the empty design give the poorest results, the box design comes closer to the shape optimized design, and this tendency strengthen when moving the interface closer to the inlet e.g. for $L = 0.35W$. Since the box design evens out the pressure due to the

Table 1. The volume of the different designs of the expansion chamber, using the abbreviations: TO = Topology Optimized, SO = Shape Optimized, ED = Empty Design, and BD-X = Box Design, with the corresponding length-to-width fraction $X = L/W$. Second row shows the volumes in relation to the Shape optimized design.

Type	TO	SO	ED	BD-0.95	BD-0.75	BD-0.55	BD-0.35
Vol (μL)	27.7	27.6	37.6	68.4	62.0	55.6	49.2
Vol/Vol(SO)	1.01	1	1.36	2.48	2.25	2.01	1.78

translation invariant properties in the reactor part, there is a limit in how fast this can happen, as reflected in the slope of the dash-dotted lines in figure 5(b). On the contrary, the optimized designs aims at homogenizing the pressure by designing the expansion-parts, and therefore their corresponding slopes are steeper than the box design. As a result, the optimized designs are most efficient in quickly producing homogeneous pressure-fields.

The hydraulic resistance $R_{\text{hyd}} = \Delta p/Q$ of the expansion-regions for all the presented designs are in the range $R_{\text{hyd}} = (1.7 - 3.7) \times 10^5 \text{ kg m}^{-4} \text{ s}^{-1}$, which is five orders of magnitude smaller than the numerically estimated $R_{\text{hyd}} \approx 2.2 \times 10^{10} \text{ kg m}^{-4} \text{ s}^{-1}$ for the micro cell culture [8].

The optimized designs possesses another advantage, since the fluid-volume of the corresponding expansions regions are significantly smaller than any of the other designs mentioned. The fluid-volume of the different expansion-regions has been calculated/measured and is presented in Table 1. Also presented in the table is the volumes relative to the Shape optimized design, and this clearly shows that extra fluid-volume is significantly higher especially for the box designs.

From the above results we conclude that the optimized designs are generally better than the alternative designs, and we will therefore in the following present a general description based on a vast range of different shape optimized designs.

Knowing now the basic shape of the height interface in the expansion region, we can now apply the right mass-conserving boundary conditions of equation (4) to the interface, and thereby improve the model upon which the following design guide is based.

5. Design guide

It is possible to match the numerically optimized geometry by simple theoretical models, which only depend significantly on the parameters W, L, \mathcal{A} , as the remaining parameters ℓ and h_1 only introduce minor corrections. By fitting the resulting interface obtained in these models for given parameters to the corresponding shaped optimized interface, we obtain an approximate parametrization which can serve as an easily applicable guide for practical design purposes.

The basic idea behind the simple models is sketched in figure 6. Given the laminar

nature of the flow, we consider an idealized narrow flow stream stretching from the inlet, across the expansion chamber, to the entrance of the main reactor. The first part of the stream, which is the lower part of figure 6a, goes along the horizontal symmetry-axis and starts at the inlet where the hydraulic damping factor is α_1 given by the height h_1 , see equation (3). Then, at the point $(x_0, y(x_0))$ the stream hits the interface, and continues horizontally to the point $(L, y(x_0))$ with hydraulic damping factor α_2 . Along all streams, the hydraulic resistance is proportional to the effective length $L_{\text{eff}} = \alpha_1 L_1 + \alpha_2 L_2$, where $L_1 = \sqrt{x_0^2 + y(x_0)^2}$ and $L_2 = L - x_0$ is the length of the first and second part of the stream, respectively. Since we seek the shape $(x_0, y(x_0))$ of the interface giving rise to the same pressure drop along the streamlines, all streamlines must have the same effective length. The specific form of the effective length, with its squares of x_0 and $y(x_0)$, then leads us to expect an expression for $y(x_0)$, or in dimensionless form, an expression for $s(\beta)$ of the form

$$s_{\text{fit}}(\beta) = 1 - \frac{\mathcal{S}_{0,P} W^2}{L^2(\mathcal{A}\sqrt{\mathcal{A}} - 1)} \left(1 - \frac{\sqrt{\beta^2 + \mathcal{C}_P^2}}{\sqrt{1 + \mathcal{C}_P^2}} \right). \quad (13)$$

The proposed expression for $s(\beta)$ is of course not exact, but by calculating the shape optimized interface for a large number of parameter values, we can fit equation (13) and make an statistical analysis of the obtained fitting parameters $\mathcal{S}_{0,P}$ and \mathcal{C}_P . The resulting explicit parametrization becomes

$$s_{\text{design}}(\beta) = 1 - \frac{2.63 W^2}{L^2(\mathcal{A}\sqrt{\mathcal{A}} - 1)} \left(1 - \frac{\sqrt{\beta^2 + 0.0729}}{1.036} \right). \quad (14)$$

This parametrization is deduced for a plug flow model, which is shown in figure 6b, while a more refined radial model, seen in figure 6c, can only be solved numerically. A comparison between the two models, is seen in figure 7. Here, the position $s(0)$ of the interface at the center axis in the simple models for a large number of parameter values is compared to that of the shape optimized model. These results show no improvement

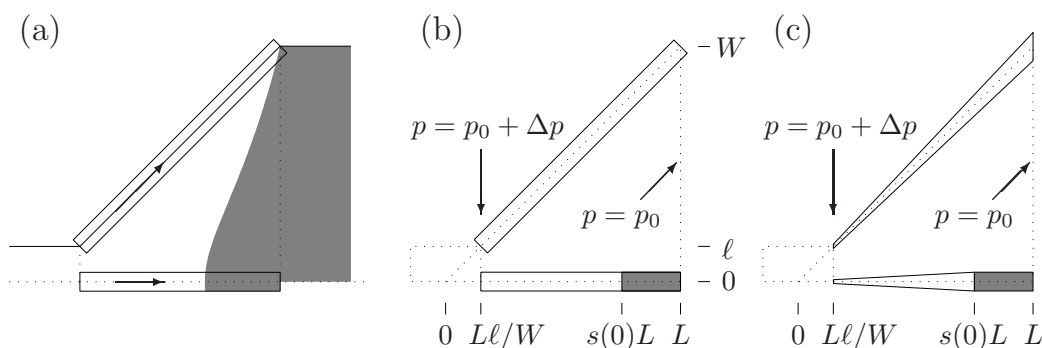


Figure 6. (a) The concept behind the models where the flow along two distinct flow stream in the expansion chamber are compared. (b) The plug flow model, and (c) the radial flow model. Also shown are the involved parameters and constraints. The gray area corresponds to regions of height h_2 .

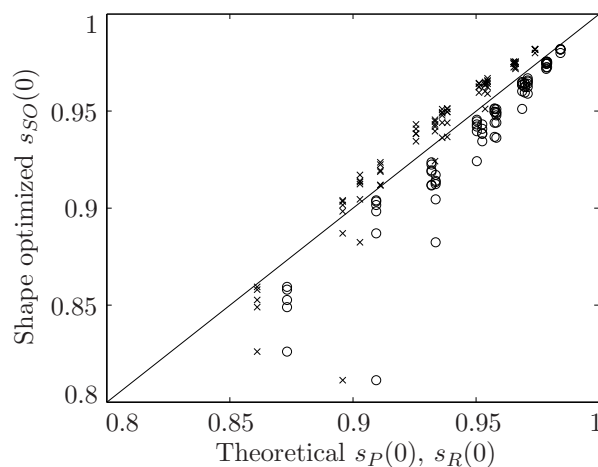


Figure 7. A comparison of the calculated beginning $s(0)$ of the transition region at the center axis between the simple model predictions and the shape optimization model. The comparison includes the simple model (crosses) and the radial model (circles), and a perfect match would lie at the diagonal (solid line).

by the radial model, and therefore it is adequate to base the design guide of equation 14 on the plug model.

The design guide does generally a very good job, but it maybe worth adjusting the parameters used above ($\mathcal{S}_{0,P} = 2.63$, and $\mathcal{C}_P = 0.27$) if the flow-homogeneity is very crucial. The best results are obtained within the following range of parameters: $0.4 < L/W < 1.6$, $6.25 < \mathcal{A} < 16$, $\ell/W < 0.2$, and $h_1/W < 0.1$. This range should be met naturally for most applications, and since we have based this work on creeping flow, the Reynolds number of the perfusion flow should be kept below or around unity.

In all, we thus find that equation 14 can serve as a fairly accurate design guide, applicable for designing microfluidic bio-reactors.

6. Direct 3D simulation

Up to this point we have relied on the 2D flow model based on the Brinkman-Darcy equation. To validate this approach and test the guideline parametrization of equation (14), we made a full 3D direct numerical simulations of the derived bio-reactor design for a given set of parameters. The resulting system was modeled and solved in COMSOL using a ordinary laptop computer, and the solution is presented in figure 8, where both iso-surfaces of the pressure and streamlines are showed inside the computational domain.

Similar to the earlier quasi 3D solutions of the optimized design, the pressure is nicely homogenized in the region of main reactor height, and also the streamlines arrange parallel through the main reactor. We take these results as a clear validation of the lubrication approach used in this work. Besides, the homogeneous flow produced by the design in figure 8 emphasizes the value of derived design and the parameterizations

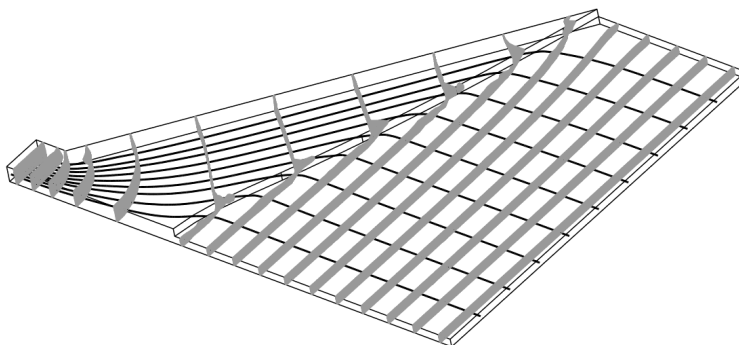


Figure 8. Direct 3D numerical solution of an optimized design following the parametrization guide of equation 14. Pressure iso-surfaces are gray, and streamlines are solid lines. Parameters are $L = 0.95W$, $\ell = 0.1W$, $h1 = 0.04W$, and $\mathcal{A} = 4$.

guide of equation (14).

7. Conclusion

To increase the utilization of continuously feed microfluidic bio-reactors, we have optimized the flow-geometry of the reactor as to expose all immobilized organisms or substances to a very homogeneous flow field. From this we have derived a general guideline of how to construct the optimal design for a broad range of reactor-dimensions.

As the overall height of the system is much smaller than the remaining physical dimensions, the 3D fluid flow can essentially be described as a 2D fluid flow using a lubrication theory approach, where an additional volume-force arise from the viscous drag by the upper and lower channel-walls.

In this work we first achieved an optimal flow-geometry by applying the free-form method of topology optimization. As the resulting shape in the design had a simple single-connected topology, we subsequently applied shape-optimization to obtain the different optimal geometries for various reactor-dimensions. From this analysis, we have constructed a general parametrization of an optimal design, which has been validated by direct 3D simulations.

The design produces the homogeneous flow with a very low pressure drop, and this will dramatically reduce the power needed to drive the perfusion flow through the system. This opens the possibilities of driving the perfusion in radically new ways e.g. by buoyancy effects. Furthermore the fluid-volume of the flow-homogenizing design is minimized, which is essential when dealing with very limited fluid-samples.

Besides applying the design to bio-reactors, it is also applicable to many other microfluidics system requiring perfusion of a large squared area, such as DNA and protein microarrays and investigation of tissue slices using fluorescent in situ hybridization or immuno chemistry, where samples typically are limited.

Acknowledgments

F. O. was supported by the European Commission through the project SMART Bio-MEMS grant No. IST-016554, and by the Carlsberg Foundation, Denmark, grant No. 2006_01_0580.

References

- [1] J. El-Ali, P. K. Sorger and K. F. Jensen, *Cells on chips*, Nature, **442**, 403-411 (2006).
- [2] N. Li Jeon, H. Baskaran, S. K. Dertinger, G. M. Whitesides, L. Van de Water, and M. Toner, *Neutrophil chemotaxis in linear and complex gradients of interleukin-8 formed in a microfabricated device*, Nat. Biotechnol., **20**, 826-830 (2002).
- [3] P. J. Hung, P. J. Lee, P. Sabounchi, N. Aghdam, R. Lin, and L. P. Lee, *A novel high aspect ratio microfluidic design to provide a stable and uniform microenvironment for cell growth in a high throughput mammalian cell culture array*. Lab Chip, **5**, 44-48 (2005).
- [4] P. J. Hung, P. J. Lee, P. Sabounchi, R. Lin, and L. P. Lee, *Continuous perfusion microfluidic cell culture array for high-throughput cell-based assays*, Biotechnol. Bioeng., **89**, 1-8 (2005).
- [5] H. Yu, I. Meyvantsson, I. A. Shkel, and D. J. Beebe, *Diffusion dependent cell behavior in microenvironments*. Lab Chip, **5**, 1089-1095 (2005).
- [6] S. Petronis, M. Stangegaard, C. Christensen, and M. Dufva, *Transparent polymeric cell culture chip with integrated temperature control and uniform media perfusion*, Biotechniques, **40**, 368-376 (2006).
- [7] N. Korin, A. Bransky, U. Dinnar, et al., *A parametric study of human fibroblasts culture in a microchannel bioreactor*, Lab on a Chip, **7** (5), 611-617 (2007).
- [8] M. Stangegaard, S. Petronis, A.M. Jørgensen, C.B.V. Christensen, and M. Dufva, *A Biocompatible Micro Cell Culture Chamber (μ CCC) for the Culturing and On-line Monitoring of Eukaryote Cells*, Lab on a Chip, **6**, 1045 - 1051 (2006).
- [9] M. Stangegaard, Z. Wang, J. P. Kutter, M. Dufva, and A. Wolff, *Whole genome expression profiling using DNA microarray for determining biocompatibility of polymeric surfaces*, Molecular Biosystems, **2**, 421-428 (2006).
- [10] Henrik Bruus, *Theoretical Microfluidics*, Oxford Master Series in Condensed Matter Physics, Oxford University Press, New York (2008).
- [11] T. Borrvall and J. Petersson, *Topology optimization of fluids in Stokes flow*, International Journal for Numerical Methods in Fluids **41**:77-107 (2003).
- [12] M. P. Bendsøe and O. Sigmund, *Topology Optimization-Theory, Methods and Applications*. Springer: Berlin, (2003).
- [13] Bendsøe MP, Kikuchi N. *Generating optimal topologies in structural design using a homogenization method*, Computer Methods in Applied Mechanics and Engineering **71**(2):197-224 (1988).
- [14] L. H. Olesen, F. Okkels, and H. Bruus, Int. J. Num. Meth. Eng. **65**, 975 (2006).
- [15] F. Okkels and H. Bruus, *Scaling behavior of optimally structured catalytic microfluidic reactors*, Phys. Rev. E **75**, 016301 (2007).
- [16] The MathWorks, Inc. (www.mathworks.com).
- [17] COMSOL AB (www.comsol.com).
- [18] M. Krishnan, N. Agrawal, M. A. Burns and V. M. Ugaz, *Reactions and Fluidics in Miniaturized Natural Convection Systems*, Anal. Chem. **76**, 6254-6265 (2006).
- [19] The routine `fminbnd` in MATLAB version 7 (R14).
- [20] The routine `fminsearch` in MATLAB version 7 (R14).
- [21] The hydraulic resistance R_{hyd} of a given channel segment is the proportionality factor between the related pressure-drop Δp and the flow-rate Q : $\Delta p = R_{\text{hyd}} Q$.

[22] The parameters used are all combinations of: $W = 0.01$ m, $L/W = \{0.8, 1, 1.2, 1.4, 1.6\}$,
 $\ell/W = \{0.05, 0.1, 0.2\}$, $h_1/\ell = \{0.1, 0.4\}$, and $\mathcal{A} = \{6.25, 9, 12.25, 16\}$.